J Electr Eng Technol.2015; 10(3): 1363-1369
http://dx.doi.org/10.5370/JEET.2015.10.3.1363

ISSN(Print) 1975-0102
ISSN(Online) 2093-7423

Dynamic Droop-based Inertial Control of a Wind Power Plant

Min Hwang*, Yeong-Han Chun, Jung-Wook Park*** and Yong Cheol Kang†**

Abstract – The frequency of a power system should be maintained within the allowed limits for stable operation. When a disturbance such as generator tripping occurs in a power system, the frequency is recovered to the nominal value through the inertial, primary, and secondary responses of the operating synchronous generators (SGs). However, for a power system with high wind penetration, the system inertia will decrease significantly because wind generators (WGs) are operating decoupled from the power system. This paper proposes a dynamic droop-based inertial control for a WG. The proposed inertial control determines the dynamic droop depending on the rate of change of frequency (ROCOF). At the initial period of a disturbance, where the ROCOF is large, the droop is set to be small to release a large amount of the kinetic energy (KE) and thus the frequency nadir can be increased significantly. However, as times goes on, the ROCOF will decrease and thus the droop is set to be large to prevent over-deceleration of the rotor speed of a WG. The performance of the proposed inertial control was investigated in a model system, which includes a 200 MW wind power plant (WPP) and five SGs using an EMTP-RV simulator. The test results indicate that the proposed scheme improves the frequency nadir significantly by releasing a large amount of the KE during the initial period of a disturbance.

Keywords: Wind power plant control, Inertial control, Rate of change of frequency, Droop control

1. Introduction

The frequency of a power system should be maintained within the allowed limits to supply high-quality electricity. The system frequency interrelated to the active power balance between generation and consumption. In order to balance of active power, SGs with spinning reserve provide the frequency control such as the inertial response, the primary control, and the secondary control [1].

Since wind energy has reached grid parity, the global installed capacity of WGs increased to 199 GW as of 2010 and it is expected to increase to 832 GW by 2020 [2]. Accordingly, global wind energy penetration will reach to 8.3 % and 15.8 % in 2020 and 2030, respectively. In 2050, all electrical energy in the EU will be supplied by renewable energy sources and half of them will come from wind energy [3].

Variable speed WGs, which have been used widely, are operating in a maximum power point tracking (MPPT) control mode [4]. The MPPT control of WGs does not respond to the system frequency but the wind speed. This causes larger frequency drop and consequently jeopardizes the reliability of the power system. Therefore, the WGs should provide frequency support controllability as the conventional SGs.

To do this, WPP inertial control schemes based on the power system frequency have been reported [6-11]. The auxiliary loops, i.e. a rate of change of frequency (ROCOF) loop [6, 7], a droop loop with a ROCOF loop [8-10], and a droop loop with the maximum ROCOF loop [11], were proposed to release the kinetic energy (KE) stored in the rotating mass of WGs.

During the initial period of a disturbance, the ROCOF has a large value and the ROCOF loop is dominant since the ROCOF loop generates the power reference depending on the ROCOF [6, 7]. However, because of provision of active power from the SGs, the ROCOF decreases with time and thus, active power from the ROCOF loop will decrease. Furthermore, the ROCOF loop gives a negative contribution in frequency support after the frequency rebound. On the other hand, the droop loop generates additional power reference in proportion to the difference between the system frequency and the nominal frequency. The ROCOF loop is dominant at the initial period of a disturbance whilst the droop loop is dominant around the frequency nadir. The combination of the ROCOF loop and the droop loop has been suggested for mitigating the negative contribution from ROCOF loop and releasing a large amount of power until the frequency nadir [8]. The droop gain is adjusted depending on the rotor speed of a WG to release more KE [9] and it is dynamically controlled by using a fuzzy controller to maintain the power system frequency [10]. The maximum ROCOF is used to overcome the negative impact of the ROCOF

† Corresponding Author: Dept. of Electrical Engineering, WeGAT Research Center, and Smart Grid Research Center, Chonbuk National University, Korea. (yckang@jbnu.ac.kr)
* Dept. of Electrical Engineering and WeGAT Research Center, Chonbuk National University, Korea. (skyway333@jbnu.ac.kr)
** Dept. of Electrical Engineering, Hongik University, Korea. (yhchun @hongik.ac.kr)
*** School of Electrical and Electronic Engineering, Yonsei University, Seoul, Korea. (jungpark@yonsei.ac.kr)
Received: November 17, 2014; Accepted: January 22, 2015

loop [11].

A dynamic droop-based inertial control for a WPP has been proposed [12] and this paper describes the extended study results of [12]. In the dynamic droop-based inertial control, at the initial period of a disturbance, where the ROCOF is large, the droop is set to be small to release a large amount of the KE. However, as times goes on, the ROCOF will decrease and thus the droop is set to be large. The performance of the proposed control algorithm was investigated in a model system, which consists of an aggregated 200 MW doubly-fed induction generator (DFIG)-based WPP and five SGs under various conditions using an EMTP-RV simulator.

2. Dynamic Droop-based Inertial Control for a WPP

This paper aims at increasing the frequency nadir by releasing a large amount of the KE of a WPP during the initial period of a disturbance. The proposed inertial control uses a droop loop, the gain of which is changed based on the ROCOF. This subsection describes the conventional inertial control scheme [8] briefly and the proposed inertial control scheme.

2.1 Conventional inertial control of a DFIG [8]

Fig. 1 shows the auxiliary loops of the conventional inertial control of a DFIG [8]. P_{ref} consists of P_0, ΔP, and ΔP_{in}. ΔP in Fig. 1 is determined by the product of the frequency deviation and R, i.e.,

$$\Delta P = -\frac{1}{R}(f_{sys} - f_{nom}) \tag{1}$$

where f_{sys} is the system frequency and f_{nom} is 60 Hz.

On the other hand, the reference from the bottom loop, ΔP_{in}, is determined by the product of the ROCOF and K, i.e.

$$\Delta P_{in} = K \times f_{sys} \times \frac{df_{sys}}{dt} \tag{2}$$

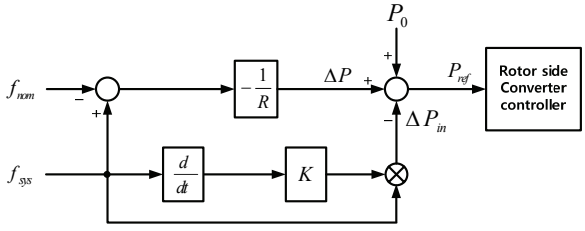

f_{nom}: nominal frequency
R: droop gain
P_0: reference for MPPT
ΔP_{in}: reference from bottom loop
f_{sys}: system frequency
k: gain of the ROCOF loop
ΔP: reference from top loop
P_{ref}: reference for the RSC

Fig. 1. Conventional inertial control loops of a DFIG [8]

Therefore, the relationship between the rotor speed of a WG, ω_r and the difference between the mechanical power, P_m, and the electrical output power, P_e is represented by

$$P_m - P_e = P_m - \left(P_0 + \Delta P - \Delta P_{in}\right) = J\omega_r \frac{d\omega_r}{dt} \tag{3}$$

where J is the moment of inertia of the rotor in kg·m^2.

When a disturbance occurs, ΔP and ΔP_{in} increase and thus the KE is released from the rotating mass and thus the rotor speed will decrease.

2.2 Proposed inertial control of a DFIG

Fig. 2 shows the configuration of the proposed inertial control scheme. The proposed control scheme uses the droop loop only. However, to release more KE immediately after a disturbance, the dynamic droop, $R(t)$, changes with the ROCOF and thus the power reference $\Delta P_{dynamic}$ is determined by

$$\Delta P_{dynamic} = -\frac{1}{R(t)}(f_{sys} - f_{nom}) \tag{4}$$

The relationship between ω_r and power P_m, and P_e can be obtained from

$$P_m - \left(P_0 + \Delta P_{dynamic}\right) = J\omega_r \frac{d\omega_r}{dt} \tag{5}$$

If a disturbance occurs, the system frequency decreases. In order to enhance the frequency nadir, releasing a large amount of power is essential during the initial period of a disturbance. To do this, the proposed inertial control uses the dynamic droop, which is converted from the ROCOF.

There are many ways that transform the ROCOF into $R(t)$. For convenience, this paper uses the simple relationship between $R(t)$ and ROCOF as shown in Fig. 3.

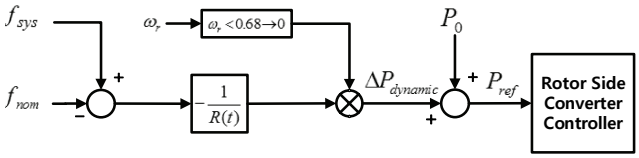

Fig. 2. Proposed inertial control loop of a DFIG

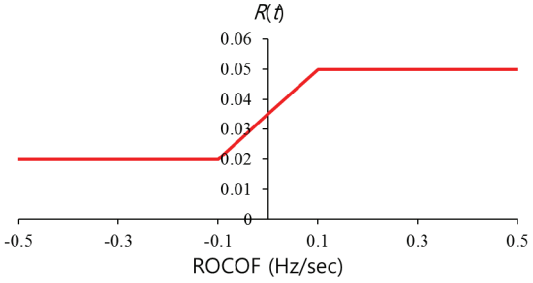

Fig. 3. Relationship between $R(t)$ and the ROCOF

If the ROCOF is smaller than −0.1, the $R(t)$ is set to 0.02. In addition, for the ROCOF from −0.1 to 0.1, $R(t)$ is set to be proportional from 0.02 to 0.05. Finally, for the ROCOF larger than 0.1, $R(t)$ is set to 0.05, which is the same value as that of the SGs. Note that the relationship between the ROCOF into $R(t)$ depends on the application purpose.

As shown in Fig. 2, to prevent over-deceleration of the WG, the proposed inertial control includes a disable loop, which is activated if the rotor speed of a WG reaches 0.68 pu. This loop will help to avoid stall of a WG.

3. Model system

Fig. 4 shows a model system used to investigate the performance of the proposed inertial control. The model system consists of the five SGs of 900 MW, a load of 600 MW and 5 MVAr, and a 200 MW DFIG-based WPP. The following subsections will describe the detailed information on the SGs and the WPP.

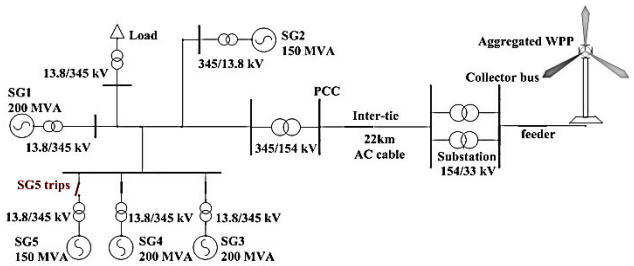

Fig. 4. Model system

3.1 Synchronous generators

The five SGs including two 150 MVA SGs and three 200 MVA SGs are connected to the model system. All SGs are using the IEEEG1 steam governor model and the droop gains are set to 5 %. The steam turbine governor model and coefficients of the governor are described in Fig. 5 and Table 1, respectively.

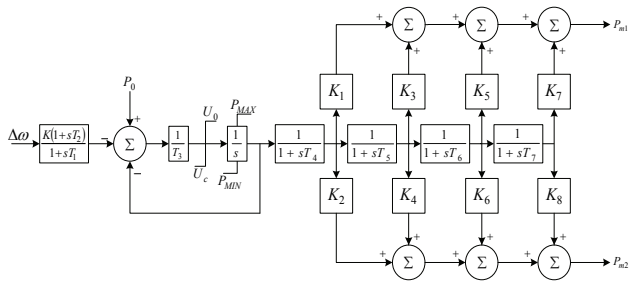

Fig. 5. IEEEG1 steam governor model

Table 1. Coefficients of the IEEEG1 model

K	T_1	T_2	T_3	U_o	U_c	P_{MAX}	P_{MIN}	T_4	K_1
20	0.1	0	0.25	0.3	−0.5	1	0.33	0.3	0.3
K_2	T_5	K_3	K_4	T_6	K_5	K_6	T_7	K_7	K_8
0	10	0.4	0	0.4	0.3	0	0	0	0

3.2 Wind power plant

An aggregated DFIG-based WPP is modeled in the model system. Fig. 6 shows the power curve of the WPP, where the cut-in, rated, and cut-out speeds are 4 m/s, 11 m/s, and 25 m/s, respectively. The MPPT power reference of the DFIG is set to be $k_g\omega_r^3$ as in [13]. In this paper, the operating range of the rotor speed of the DFIG is set to 0.68−1.33 pu for reliable operation.

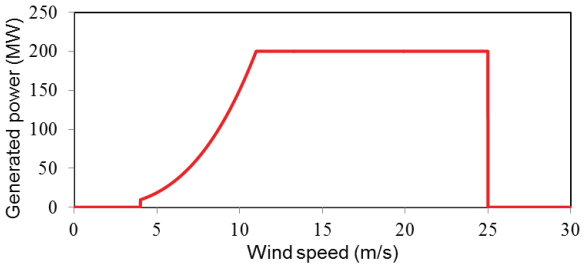

Fig. 6. Power curve of the WPP

4. Case studies

As a disturbance, SG5, which is supplying 100 MW, is assumed to be tripped out at 30s. The test results for the two cases of 8 m/s and 11m/s will be shown in this subsection. The performance of the proposed control algorithm is compared with those of the fixed droop only, the fixed droop with the ROCOF, and the 'without (w/o) inertial control'. R for the fixed droop only and the fixed droop with the ROCOF is set to 5 % [14].

To compare the performance of the inertial control algorithms, the nadir based frequency responses (NBFR), which is defined by the amount of the tripped generator to the nadir, as well as the frequency nadir, are evaluated. It assumes that WGs are operating in the MPPT mode prior to the disturbance and this means WGs has no reserve power.

4.1 Case 1: wind speed of 8 m/s, wind penetration of 12.8 %

Fig. 7 shows the results for case 1. Fig. 7(a) shows the system frequencies. The frequency nadirs for 'w/o inertial control', fixed droop only, fixed droop with ROCOF, and dynamic droop are 58.83 Hz, 59.32 Hz, 59.36 Hz, and 59.47 Hz, respectively. The frequency nadir of the proposed control appeared the highest and latest among them. In addition, the NBFRs for 'w/o inertial control', fixed droop only, fixed droop with ROCOF, and dynamic droop are 8.56 MW/0.1 Hz, 14.86 MW/0.1 Hz, 15.56 MW/0.1 Hz, and 19.13 MW/0.1 Hz, respectively. This means the NBFR of the proposed control is larger than

those of the other inertial control schemes.

Figs. 7(b) and 7(c) show the ROCOF and corresponding $R(t)$, which is obtained by using Fig. 3. As expected, the ROCOF is larger than -0.1 at the initial period of a disturbance and thus the $R(t)$ is set to 0.02 from Fig. 3. $R(t)$ is kept to 0.02 until the ROCOF reaches -0.1. Afterwards, $R(t)$ increases as the ROCOF increases. We can see that $R(t)$ reaches 0.035 when the ROCOF converges nearly zero.

Fig. 7(d) shows additional power. The peak values of additional power for fixed droop only, fixed droop with ROCOF, and dynamic droop are 53.76 MW, 52.93 MW, and 69.96 MW, respectively. As expected, because $R(t)$ is set to be small as shown in Fig. 7(c), the dynamic droop releases a large amount of additional power immediately after a disturbance. As time goes on, additional power decreases in accordance with the reduction of the ROCOF and the frequency deviation. It will converge because the frequency deviation becomes constant as time goes on. This is because the automatic generation control (AGC) to eliminate the steady state error is not included in this paper and the steady state error of the frequency is inevitable. If the AGC scheme is included and the frequency is completely recovered to the nominal value, the additional power will be zero.

As shown in Figs. 7(e) and 7(f), P_0 decreases with time because the rotor speed of a WG decreases due to the released KE for the inertial control (see Fig. 7(f)). The reduction of the rotor speed of the proposed control is the largest since additional power for the proposed control is the largest as shown in Fig. 7(d). P_0 for the dynamic droop decreases significantly with time compared with those of the other inertial control. The reduction in P_0 helps to avoid over-deceleration of a WG.

Fig. 7(g) shows P_{ref}, which is the sum of additional power of Fig. 7(d) and P_0 of Fig. 7(e). The maximum value of P_{ref} for 'w/o inertial control', fixed droop only, fixed droop with ROCOF and dynamic droop are 79.55 MW, 122.26 MW, 121.34 MW, and 144.49 MW, respectively. Although P_0 for the proposed control decreases more than the other control schemes, additional power for the proposed control releases a large amount of the KE particularly in the early stage during the disturbance. Therefore, the proposed scheme can increase the frequency

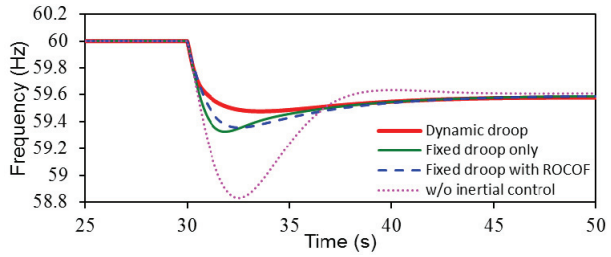

(a) System frequency

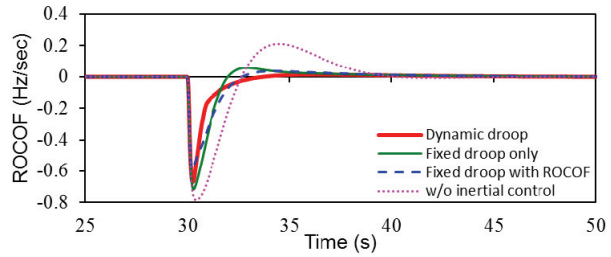

(b) ROCOF

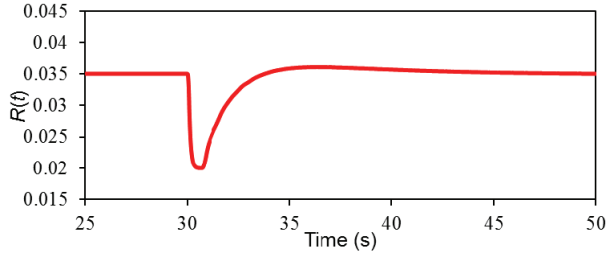

(c) Dynamic droop

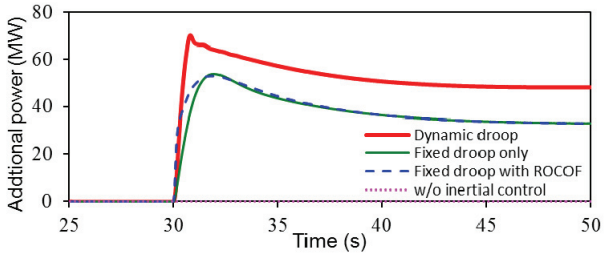

(d) Additional power

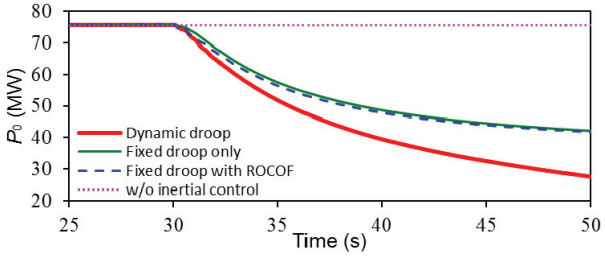

(e) P_0

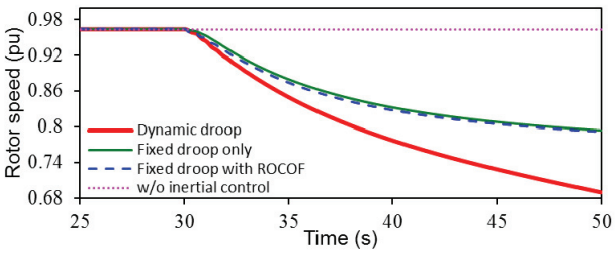

(f) Rotor speed

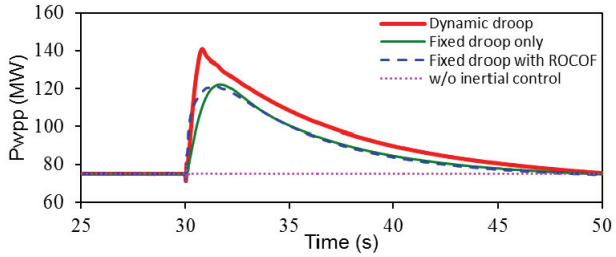

(g) P_{ref}

Fig. 7. Results for case 1

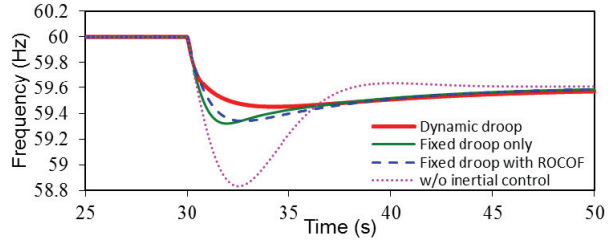

(a) System frequency

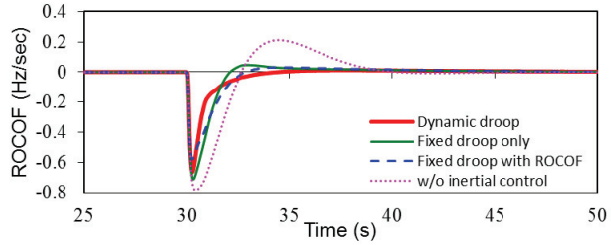

(b) ROCOF

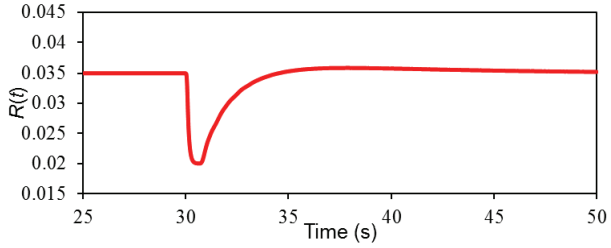

(c) Dynamic droop

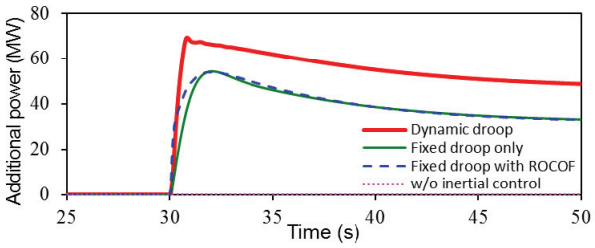

(d) Additional power

nadir significantly.

4.2 Case 2: wind speed of 11 m/s, wind penetration of 33.3 %

Fig. 8 shows the results for case 2, which is the same condition case 1 except for the wind speed. As shown in Fig. 8(a), the frequency nadirs for 'w/o inertial control', fixed droop only, fixed droop with ROCOF, and dynamic droop are 58.83 Hz, 59.32 Hz, 59.34 Hz, and 59.45 Hz, respectively. In addition, the NBFRs for 'w/o inertial control', fixed droop only, fixed droop with ROCOF, and dynamic droop are 8.56 MW/0.1Hz, 14.71 MW/0.1Hz, 15.15 MW/0.1Hz, and 18.21 MW/0.1Hz, respectively. As in case 1, for the proposed control, the frequency nadir appears the highest and latest, and the NBFR is the largest.

As shown in Figs 8(b) to 8(c), the ROCOF varies larger than -0.1 at initial period of a disturbance, and thus the $R(t)$ is kept to be 0.02 until the ROCOF exceeds -0.1. Thereafter, $R(t)$ increases with the ROCOF and converges 0.035 when the ROCOF becomes nearly zero.

For the proposed control, additional power increases immediately after disturbance since $R(t)$ is set to be small during the initial period of a disturbance (see Fig. 8(d)). Afterwards, it decreases depending on the reduction of the ROCOF and the frequency deviation.

As shown in Figs. 8(e) and 8(f), P_0 for the proposed control decreases with time because the proposed control releases a large amount of the KE and thus the rotor speed of the WG decreases significantly.

The maximum value of P_{ref} for 'w/o inertial control', fixed droop only, fixed droop with ROCOF, and dynamic droop are 197.03 MW, 239.14 MW, 238.39 MW, and 257.26 MW, respectively (see Fig. 8(g)).

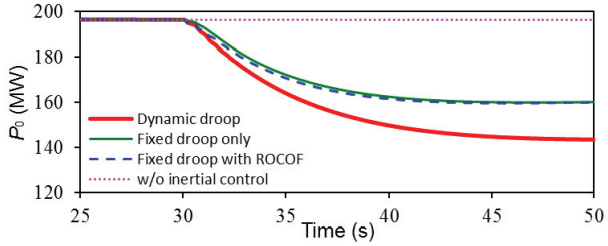

(e) P_0

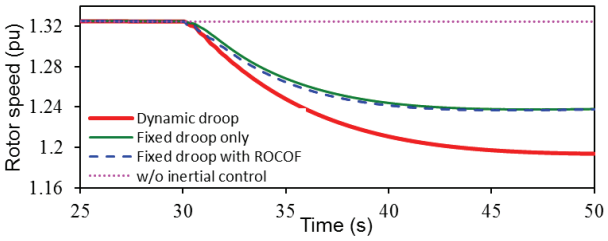

(f) Rotor speed

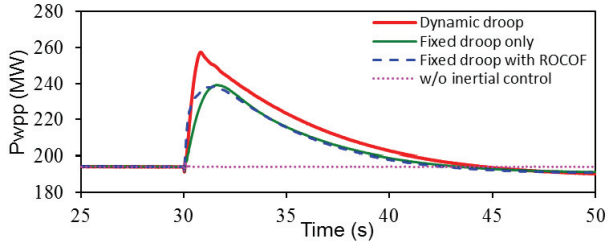

(g) P_{ref}

Fig. 8. Results for case 2

5. Conclusion

This paper proposes an inertial control algorithm of a DFIG-based WPP using the dynamic droop. The proposed inertial control determines the droop based on the ROCOF. To release a large amount of the KE during the initial period of a disturbance, the droop is set to be small when

the ROCOF is large. On the other hand, to prevent over-deceleration of the rotor speed of a WG, the droop is set to be large when the ROCOF is small.

The test results clearly indicate that the proposed inertial control can release the KE more than the conventional inertial control. Therefore, the frequency nadir and the NBFR are increased more than the conventional inertial control schemes.

Acknowledgements

This work was supported partly by the National Research Foundation of Korea (NRF) grant funded by the Korea government (MSIP) (2010-0028509) and partly by Power Generation & Electricity Delivery Core Technology Program of the Korea Institute of Energy Technology Evaluation and Planning (KETEP) granted financial resource from the Ministry of Trade, Industry & Energy, Korea (20141020402340).

References

[1] T. Ackermann, *Wind Power in Power System*, 2nd Edition, England, John Wiley & Sons, Ltd, 2012.

[2] *Global wind energy outlook 2012*, Global Wind Energy Council, Nov. 2012.

[3] The European Wind Energy Association, *EU Energy policy to 2050*, EWEA, 2011.

[4] O. Anaya-lara, N. Jenkins, J. Ekanayake, P. Cartwright, and M. Hughes, *Wind Energy Generation Modeling and Control*, John Wiley & Sons, Ltd, 2009.

[5] S.-E. Lee, D.-J. Won, and I.-Y. Chung, "Operation scheme for a wind farm to mitigate output power variation," *Journal of Electrical Engineering & Technology,* vol. 7, no. 6, 2012, pp. 869-875.

[6] J. Ekanayake, L. Holdsworth, and N. Jenkins, "Control of DFIG wind turbines" *IEEE Power Engineer*, vol. 17, no. 1, 2003, pp. 28-32.

[7] J. Ekanayake and N. Jenkins, "Comparison of the response of doubly fed and fixed-speed induction generator wind turbines to changes in network frequency," *IEEE Transaction on Energy conversion*, vol. 19, no. 4, 2004, pp. 800-802.

[8] J. Morren, S. Haan, W. L. Kling, and J. A. Ferreira, "Wind turbines emulating inertia and supporting primary frequency control," *IEEE Transaction on Power systems*, vol. 21, no. 1, 2006, pp. 433-434.

[9] J. Lee, J. Kim, Y.-H. Kim, Y.-H. Chun, S.-H. Lee, J.-K. Seok, and Y. C. Kang, "Rotor speed-based droop of a wind generator in a wind power plant for the virtual inertial control," *Journal of Electrical Engineering & Technology,* vol. 8, no. 5, 2013, pp. 742-749.

[10] R. L. Josephine and S. Suja, "Estimating PMSG wind turbines by inertia and droop control schemes with intelligent fuzzy controller in Indian development," *Journal of Electrical Engineering & Technology*, vol. 9, no. 4, 2014, pp. 1196-1201.

[11] H. Lee, J. Kim, D. Hur, and Y. C. Kang, "Inertial control of a DFIG-based wind power plant using the maximum rate of change of frequency and the frequency deviation," *Journal of Electrical Engineering & Technology*, vol. 10, no. 2, 2015, pp. 496-503.

[12] M. Hwang, H. Lee, Y.-H. Chun, and Y. C. Kang, "Dynamic droop-based inertial control of a wind power plant," *20th ICEE*, 2014, pp. 210-212.

[13] B. Shen, B. Mwinyiwiwa, Y. Zhang, and B. Ooi, "Sensorless Maximum Power Point Tracking of Wind by DFIG Using Rotor Position Phase Lock Loop," *IEEE Transaction on Power Electronics*, vol. 24, no. 4, 2009, pp. 942-951.

[14] I.D. Margaris, S.A. Papathanassiou, N.D. Hatziargyriou, A. D. Hansen, and P. Sørensen, "Frequency control in autonomous power systems with high wind power penetration," *IEEE Transaction on Sustainable Energy*, vol. 3, no. 2, 2012, pp. 189-199.

Min Hwang He is currently an undergraduate student at Chonbuk National University, Korea. He is also an assistant researcher at the Wind energy Grid-Adaptive Technology (WeGAT) Research Center supported by the Ministry of Science, ICT, and Future Planning (MSIP), Korea. His research interests include the development of wind energy grid integration techniques.

Yeong-Han Chun He received his B.S. and M.S. degrees from Seoul National University, Korea, in 1983 and 1985, respectively, and his Ph.D. degree from Tokyo University, Japan, in 1997. He was with the Korea Electro-technology Research Institute (KERI) from 1985 to 2002, and joined Hongik University, where he is currently a Professor of Electrical Engineering. His research interests are power system control and stability.

Jung-Wook Park He received the B.S. degree (summa cum laude) from the Department of Electrical Engineering, Yonsei University, Seoul, Korea in 1999, and the M.S.E.C.E. and Ph.D. degrees from the School of Electrical and Computer Engineering, Georgia Institute of Technology, Atlanta, USA in 2000 and 2003, respectively. He is currently an Associate Professor in the School of Electrical and Electronic Engineering, Yonsei University, Seoul, Korea.

Yong Cheol Kang He received his B.S., M.S., and Ph.D. degrees in the Department of Electrical Engineering from Seoul National University, Korea, in 1991, 1993, and 1997, respectively. He has been with Chonbuk National University, Korea, since 1999. He is currently Professor at the Department of Electrical Engineering, Chonbuk National University, Korea, and the director of the WeGAT Research Center. He is also with the Smart Grid Research Center at Chonbuk National University. His research interests include the development of new protection and control systems for wind power plants and the enhancement of wind energy penetration levels.